PERGAMON

International Journal of Heat and Mass Transfer 45 (2002) 1513–1523

International Journal of HEAT and MASS TRANSFER

www.elsevier.com/locate/ijhmt

Modified theoretical models of film condensation in horizontal microfin tubes

H.S. Wang [a], H. Honda [a,*], S. Nozu [b]

[a] *Institute of Advanced Material Study, Kyushu University, Kasuga, Fukuoka 816-8580, Japan*
[b] *Department of Systems Engineering, Okayama Prefectural University, Souja, Okayama 719-1197, Japan*

Received 27 December 2000; received in revised form 13 June 2001

Abstract

The previously proposed theoretical models of film condensation in horizontal microfin tubes have been modified to describe the characteristics of condensing two-phase flow more accurately. The stratified flow regime and the annular flow regime were considered. For the stratified flow regime, the previously proposed theoretical model was modified to take account of the curvature of stratified condensate due to the surface tension force. For the annular flow regime, a more accurate expression for the interfacial shear stress was incorporated. Generally, the modified theoretical models predicted a lower circumferential average heat transfer coefficient than the previously proposed ones. Comparison of the theoretical predictions with available experimental data for six tubes and five refrigerants revealed that a good agreement (r.m.s error of less than 21.1%) was obtained for all cases when the higher of the two theoretical predictions were adopted as the calculated value.

Keywords: Condensation; Stratified flow model; Annular flow model; Helical microfin tube; Refrigerants

1. Introduction

Horizontal microfin tubes have been commonly used in air conditioners due to their high heat transfer performance. Many experimental studies on the effects of fin geometry, tube diameter, refrigerant, oil, etc., on the condensation heat transfer and pressure drop of the microfin tubes have been reported in the recent literature. Webb [1] and Newell and Shah [2] have given comprehensive reviews of relevant literature. Cavallini et al. [3] and Shikazono et al. [4] have developed empirical equations of the circumferential average heat transfer coefficient. Yang and Webb [5] and Nozu and Honda [6], respectively, proposed the semi-empirical model and the annular flow model of film condensation in microfin tubes that considered the combined effects of vapor shear and surface tension forces. Honda et al. [7] proposed a stratified flow model that considered the combined effects of surface tension and gravity forces. In this model the vapor–liquid interface was assumed to be flat and the height of stratified condensate was determined by extending the Taitel and Dukler model [8] for a smooth tube to a microfin tube. Honda et al. [7] compared the theoretical predictions of the circumferential average heat transfer coefficient α_m by the annular flow model [6] and the stratified flow model [7] with available experimental data for five refrigerants and five tubes. According to the result, the annular flow model predicted a considerably higher α_m than the measured value at high quality χ. This was probably due to the overestimation of the interfacial shear stress acting on the condensate film. While a better agreement (within $\pm 20\%$) was obtained as χ decreased, this model predicted a considerably lower α_m than the measured value (about one half) when χ decreased further and the fins were completely flooded with condensate. For R134a, R22 and R410A with $\rho_v/\rho_l > 0.05$, the predictions of the stratified flow model agreed with most of the measured values within $\pm 20\%$. However, there was a tendency to overpredict the measured value. This tendency was more significant for tubes with smaller diameter.

* Corresponding author. Tel.: +81-92-583-7787; fax: +81-92-583-7882.
E-mail address: hhonda@cm.kyushu-u.ac.jp (H. Honda).

0017-9310/02/$ - see front matter
PII: S0017-9310(01)00244-7

Nomenclature

A	cross-sectional area of tube (m^2)
Bo	Bond number ($(\rho_l - \rho_v)gd^2/\sigma$)
d	diameter at fin root (m)
d_h	hydraulic diameter (m)
d_l	equivalent diameter of liquid space ($= 4A_l/S_i$) (m)
d_o	outside diameter (m)
Δe	sum of gravitational potential and surface energy for unit length of tube (J/m)
f	friction factor
Fr	modified Froude number, $G\chi/\sqrt{\rho_v(\rho_l - \rho_v)dg}$
g	gravitational acceleration (m/s^2)
G	refrigerant mass velocity (kg/m^2 s)
h	fin height (m)
h_{fg}	specific enthalpy of evaporation (J/kg)
n	number of fins
p	fin pitch (m)
P	pressure difference between condensate and vapor (Pa)
Pr	Prandtl number
q	heat flux, W/m^2
r	radius of curvature of condensate surface in fin cross-section (m)
r_0	radius of curvature at corner of fin tip (m)
r_b	radius of curvature of condensate surface in thick film region (m)
r_r	radius of curvature at corner of fin root (m)
Re_v	vapor Reynolds number, $G\chi d/\mu_v$
S	perimeter length (m)
S_p	perimeter length of condensate surface for a fin pitch (m)
T	temperature (K)
U	velocity in axial direction (m/s)
x, y	coordinates, Fig. 1
x_b	coordinate at connecting point between thin and thick film regions, Fig. 1 (m)
x_0, x_t	coordinates at connecting points between straight and round portions of fin, Fig. 1 (m)
x_r	mid point between adjacent fins (m)
X_{tt}	Martinelli parameter
z	vertical height measured from condensate surface, Fig. 1; axial coordinate (m)

Greek symbols

α	heat transfer coefficient (W/m^2 K)
β	angle, Figs. 1(c) and (d) (°)
γ	helix angle of groove (°)
δ	condensate film thickness (m)
ε	angle, Fig. 1(d) (°)
ε_a	surface area enhancement as compared to a smooth tube
ς	wettability angle (°)
θ	fin half tip angle (°)
λ	thermal conductivity (W/m K)
μ	dynamic viscosity (Pa s)
ν	kinematic viscosity (m^2/s)
ξ	angle, Fig. 1(d) (°)
ρ	density (kg/m^3)
σ	surface tension (N/m)
τ	shear stress (Pa)
φ	angle measured from tube top (°)
χ	mass quality
ψ	angle, Fig. 1(c) (°)
ω	angle, Fig. 1(a) (°)

Subscripts

b	boundary of thin and thick film regions
c	coolant side
f	flooding point
F	frictional
i	vapor–liquid interface
l	liquid
m	circumferential average value
r	fin root, mid point at fin root
s	saturation
v	vapor
w	wall
x	local value
φ	average value for fin cross-section
1	region 1
2	region 2

For R11 and R123 with $\rho_v/\rho_l < 0.01$, the measured value agreed fairly well with the higher of the two theoretical predictions. The foregoing difference in the heat transfer characteristics between the fluids with $\rho_v/\rho_l > 0.05$ and $\rho_v/\rho_l < 0.01$ was probably due to the difference in the magnitude of vapor shear force acting on the condensate film.

Recently, in order to meet the need for more compact heat exchangers, the microfin tubes with a small outer diameter d_o have been developed for the air conditioners. Currently, the tubes with $d_o = 6$–8 mm are commonly used. The tubes with $d_o = 4$ mm have also been tested. For the stratified condensate flow in these tubes, the surface tension acts to form a curved liquid–vapor interface and the assumption of a flat vapor–liquid interface adopted by Honda et al. [7] does not hold any more. The objective of the present work is twofold. The first is to develop a modified stratified flow model in which the effect of surface tension on the vapor–liquid interface profile is taken into account. The second is to develop a more accurate expression for the interfacial shear stress which is consistent with the correlation for the frictional pressure gradient proposed by Nozu et al. [8], and to apply it to the previously proposed annular

flow model. The predictions of α_m by the newly proposed annular and stratified flow models are compared with available experimental data for six tubes and five refrigerants. Comparisons are also made with the predictions of the previously proposed annular flow model [6] and stratified flow model [7].

2. Analysis

2.1. Modified stratified flow model

Fig. 1 shows the physical model of stratified condensate flow in a horizontal microfin tube. In Fig. 1(a), the shape of stratified condensate is assumed to be a circular arc centered at O_1. The angle φ is measured from the top of the tube. The φ_s denotes the angle below which the tube is filled with stratified condensate. The coordinate z is measured vertically upward from the surface of stratified condensate at $\varphi = \varphi_s$. The tube surfaces at the angular portions of $0 \leqslant \varphi \leqslant \varphi_s$ and $\varphi_s \leqslant \varphi \leqslant \pi$ are denoted as region 1 and 2, respectively. In the angular portion just above φ_s, condensate is retained in the groove between adjacent fins by the capillary effect. As a result, a relatively thick condensate film is formed in the groove. The angle below which the condensate is retained in the groove is denoted as the flooding angle φ_f. Figs. 1(c) and (d) show the condensate profiles in the fin cross-section in the regions $0 \leqslant \varphi \leqslant \varphi_f$ and $\varphi_f \leqslant \varphi \leqslant \varphi_s$, respectively. The fin profile is assumed to be a trapezoid with round corners at the fin tip and fin root. The fin height and fin pitch are h and p, respectively, and the fin half tip angle is θ. The coordinate x is measured along the fin surface from the center of fin tip and y is measured vertically outward from the fin surface. The condensate on the fin surface is drained by the combined gravity and surface tension forces toward the fin root and then it flows down the groove by gravity. Thus the condensate film thickness δ is very small near the fin tip and it is relatively thick near the fin root. The effect of vapor shear force on the condensate flow on the fin surface is assumed to be negligible.

2.2. Profile of stratified condensate

The profile of stratified condensate is estimated by the combination of an extended Taitel and Dukler model [8] for the void fraction proposed by Honda et al. [7] and the model of interface configuration proposed by Brauner et al. [9]. The basic equation for the stratified flow with a curved interface is written as

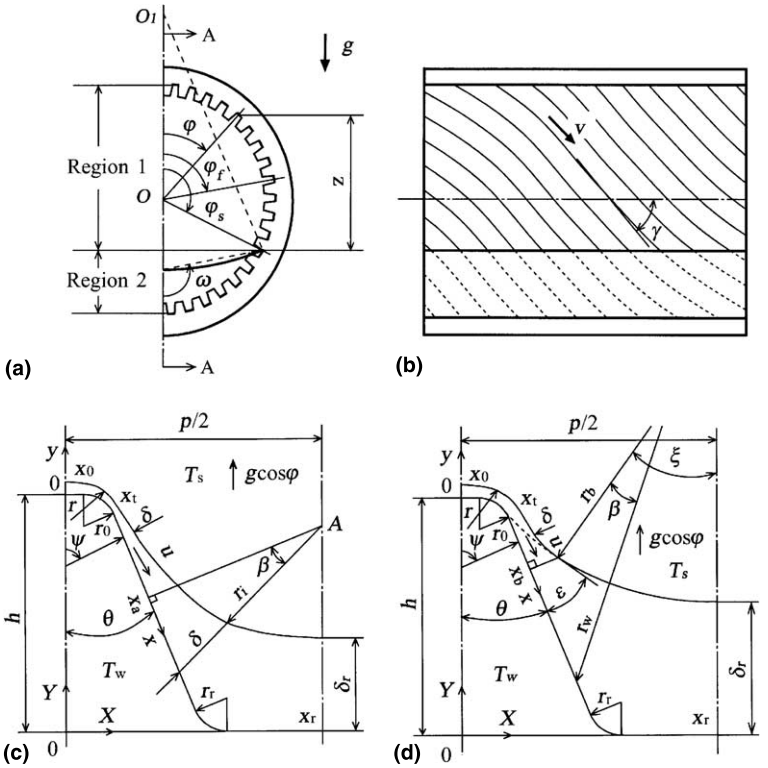

Fig. 1. Physical model and coordinates: (a) tube cross-section; (b) A–A cross-section; (c) fin cross-section ($0 \leqslant \varphi \leqslant \varphi_f$); (d) fin cross-section ($\varphi_f \leqslant \varphi \leqslant \varphi_s$).

$$f_v \frac{\rho_v U_v^2}{2} \frac{S_v}{A_v} - f_l \frac{\rho_l U_l^2}{2} \frac{S_l}{A_l} + f_i \frac{\rho_v U_v^2}{2} \left(\frac{S_i}{A_v} + \frac{S_i}{A_l} \right) = 0, \quad (1)$$

where f_v and f_l are the friction factors in regions 1 and 2, respectively, f_i is the interfacial friction factor, ρ_v and ρ_l are the densities of vapor and condensate, respectively, U_v and U_l are the velocities of vapor and condensate, respectively, A_v and A_l are the cross-sectional areas of the vapor space and condensate space, respectively, S_v and S_l are the perimeter lengths of regions 1 and 2, respectively, and S_i is the perimeter length of the interface. The values of f_v and f_l are estimated by an empirical equation for the internally finned tubes developed by Carnavos [10]. Thus they are respectively given by the following equations:

$$f_v = 0.046 \left(\frac{\rho_v d_v U_v}{\mu_v} \right)^{-0.2} \left(\frac{A}{A_n} \right)^{0.5} (\sec \gamma)^{0.75}, \quad (2)$$

$$f_l = 0.046 \left(\frac{\rho_l d_l U_l}{\mu_l} \right)^{-0.2} \left(\frac{A}{A_n} \right)^{0.5} (\sec \gamma)^{0.75}, \quad (3)$$

f_i is given by

$$f_i = 0.046 \left(\frac{\rho_v d_v U_v}{\mu_v} \right)^{-0.2}, \quad (4)$$

where d_v and d_l are the equivalent diameters of the vapor space and liquid space given by $d_v = 4A_v/(S_v + S_i)$ and $d_l = 4A_l/S_i$, respectively, A is the actual cross-sectional area of tube, A_n is the nominal cross-sectional area based on the fin root diameter d, and γ is the helix angle of the groove. The expressions for the other parameters are as follows: $U_v = GA\chi/\rho_v A_v$ $U_l = GA(1-\chi)/\rho_l A_l$, $S_v = \varepsilon_a d\varphi_s$, $S_l = \varepsilon_a d(\pi - \varphi_s)$, $S_i = d\sin\varphi_s(\pi - 2\omega)/\sin(2\omega)$

$$A_l = \frac{d^2}{4} \left[\frac{A}{A_n}(\pi - \varphi_s) + \frac{\sin(2\varphi_s)}{2} + \sin^2 \varphi_s \frac{\pi - 2\omega + \sin(4\omega)/2}{\sin^2(2\omega)} \right],$$

$$A_v = \pi d^2/4 - A_l,$$

where ε_a is the surface area enhancement as compared to a smooth tube with diameter d and ω is the angle shown in Fig. 1(a).

Following Brauner et al. [9], the interface curvature is determined by assuming the condition that the sum of gravitational potential and surface energy Δe is minimum. The Δe is given by

$$\Delta e = \frac{1}{8}(\rho_l - \rho_v) g d^3 \left[\sin^3 \varphi_s (\cot(2\omega) + \cot \varphi_s) \times \frac{\pi - 2\omega + \sin(4\omega)/2}{\sin^2(2\omega)} + \frac{2}{3}\sin^3 \varphi_s^p + \frac{8}{Bo} \left\{ \sin \varphi_s \times \frac{\pi - 2\omega}{\sin(2\omega)} - \sin \varphi_s^p + \cos \varsigma (\varphi_s - \varphi_s^p) \right\} \right], \quad (5)$$

where $Bo = (\rho_l - \rho_v) g d^2/\sigma$ is the Bond number, σ is the surface tension, φ_s^p is the value of φ_s for a plane interface ($\omega = \pi/2$), and ς is the wettability angle. It is relevant to note here that $\varsigma = 0$ for condensation. The values of φ_s and ω are obtained by solving Eqs. (1) and (5) iteratively for given conditions of d, G and χ.

2.3. Profile of thick condensate film in $\varphi_f \leqslant \varphi \leqslant \varphi_s$

In the angular portion $\varphi_f \leqslant \varphi \leqslant \varphi_s$, the condensate velocity in the thick film is considered to be very small. Thus its profile is approximated by a static meniscus that touches the fin flank (shown by a dotted line in Fig. 1(d)). Then the radius of curvature of the thick film r_b is given by

$$\frac{\sigma}{r_b} = (\rho_l - \rho_v) g z = \frac{(\rho_l - \rho_v) g d}{2} (\cos \varphi - \cos \varphi_s). \quad (6)$$

2.4. Profile of thin condensate film in $0 \leqslant \varphi \leqslant \varphi_f$

In the thin film region $0 \leqslant \varphi \leqslant \varphi_f$, δ is assumed to be sufficiently smaller than h and p. The condensate on the fin surface is drained in the x direction by the combined surface tension and gravity forces. At the same time, it is drained along the groove by the gravity force. Assuming a laminar flow, the momentum equation in the x-direction and in the direction along the groove are, respectively, written as

$$\mu_l \frac{\partial^2 u}{\partial y^2} - (\rho_l - \rho_v) g \sin \psi \cos \varphi = \frac{\partial P}{\partial x}, \quad (7)$$

$$\mu_l \frac{\partial^2 v}{\partial y^2} + (\rho_l - \rho_v) g \sin \gamma \sin \varphi = 0, \quad (8)$$

where u and v are the velocity components in the x-direction and in the direction along the groove, respectively, ψ is the angle shown in Figs. 1(c) and (d), and P is the pressure difference between the condensate and vapor due to the surface tension effect. The boundary conditions are:

$$u = v = 0 \quad \text{at} \quad y = 0, \quad (9)$$

$$\partial u/\partial y = \partial v/\partial y = 0 \quad \text{at} \quad y = \delta. \quad (10)$$

The P in Eq. (7) is given by

$$P = \sigma/r, \quad (11)$$

where r is the radius of curvature of the condensate surface in the fin cross-section. The expression for r is given by

$$\frac{1}{r} = -\frac{\partial^2 \delta/\partial x^2}{\left\{1 + (\partial \delta/\partial x)^2\right\}^{3/2}} \quad \text{for } 0 \leqslant x \leqslant x_0 \text{ and } x_t \leqslant x \leqslant x_a, \quad (12a)$$

$$\frac{1}{r}=\left\{\frac{1}{r_0}+\left(\frac{2}{r_0^2}+\frac{\delta}{r_0^3}\right)\delta+\frac{2}{r_0}\left(\frac{\partial\delta}{\partial x}\right)^2-\left(1+\frac{\delta}{r_0}\right)\left(\frac{\partial^2\delta}{\partial x^2}\right)\right/\left\{\left(1+\frac{\delta}{r_0}\right)^2+\left(\frac{\partial\delta}{\partial x}\right)^2\right\}^{3/2}\Bigg\}\quad \text{for } x_0\leqslant x\leqslant x_t \tag{12b}$$

and

$$\frac{1}{r}=\frac{r_i^2+2(\mathrm{d}r_i/\mathrm{d}\beta)^2-r_i(\mathrm{d}^2r_i/\mathrm{d}\beta^2)}{\left\{r_i^2+(\mathrm{d}r_i/\mathrm{d}\beta)^2\right\}^{3/2}}\quad \text{for } x_a\leqslant x\leqslant x_r, \tag{12c}$$

where x_0 and x_t are the connecting points between the straight and round portions of the fin surface, x_a is the coordinate at the foot of the perpendicular from point A in Fig. 1(c), x_r is the mid point at the fin root, r_0 is the radius of curvature at the corner of fin tip, r_i is the distance of the condensate surface measured from point A and β is the angle shown in Fig. 1(c). The x_a is chosen empirically so that the condition of $r_i>\delta$ is satisfied. Numerical results have shown that the heat transfer rate is little affected by x_a as long as $r_i>\delta$. For $x_a<x\leqslant x_r$, δ is defined as shown in Fig. 1(c). Since δ is very small, a linear temperature drop is assumed across the condensate film. Combining the continuity and energy equations yield

$$\rho_l\left(\frac{\partial}{\partial x}\int_0^\delta u\,\mathrm{d}y+\frac{2\sin\gamma}{d}\frac{\partial}{\partial\varphi}\int_0^\delta v\,\mathrm{d}y\right)=\frac{\lambda_l(T_s-T_w)}{h_{fg}\delta}. \tag{13}$$

Substituting the solutions of Eqs. (7) and (8) into Eq. (13) yields

$$-\frac{(\rho_l-\rho_v)g\cos\varphi}{3v_l}\frac{\partial}{\partial x}\left(\sin\psi\delta^3\right)-\frac{\sigma}{3v_l}\frac{\partial}{\partial x}\left\{\frac{\partial}{\partial x}\left(\frac{1}{r}\right)\delta^3\right\}+\frac{2(\rho_l-\rho_v)g\sin^2\gamma}{3v_l d}\frac{\partial}{\partial\varphi}\left(\sin\varphi\delta^3\right)=\frac{\lambda_l(T_s-T_{w1})}{h_{fg}\delta}. \tag{14}$$

The boundary conditions are:

$$\partial\delta/\partial\varphi=0\quad\text{at }\varphi=0, \tag{15}$$

$$\partial\delta/\partial x=\partial^3\delta/\partial x^3=0\quad\text{at } x=0 \text{ and } x_r. \tag{16}$$

2.5. Profile of thin condensate film in $\varphi_f\leqslant\varphi\leqslant\varphi_s$

For $\varphi_f\leqslant\varphi\leqslant\varphi_s$, where the condensate film is consisted of a thin film region near the fin tip and a thick film region near the fin root, the boundary conditions at the connecting point between the thin film and thick film are given by

$$\partial\delta/\partial x=\tan\varepsilon,\quad r=-r_b\quad\text{at } x=x_b, \tag{17}$$

where ε is the angle shown in Fig. 1(d).

The solution of Eq. (14) subject to the boundary conditions (15) and (16) for $0\leqslant\varphi\leqslant\varphi_f$, and (15) and (17) for $\varphi_f\leqslant\varphi\leqslant\varphi_s$ was obtained numerically by a finite difference scheme. The description of the numerical scheme is given in [7].

2.6. Wall temperature and heat transfer coefficients

For region 1, the average heat transfer coefficient for the fin cross-section α_φ is defined on the projected area basis as

$$\alpha_\varphi=\frac{2}{p}\int_0^{x_r}\alpha_x\,\mathrm{d}x=\frac{2\lambda_l}{p}\int_0^{x_r}\frac{1}{\delta}\,\mathrm{d}x, \tag{18}$$

where $\alpha_x=\lambda_l/\delta$ is the local heat transfer coefficient. The average heat transfer coefficient for region 1, α_1, is defined on the projected area basis as

$$\alpha_1=\frac{1}{\varphi_s}\int_0^{\varphi_s}\alpha_\varphi\,\mathrm{d}\varphi=\frac{2\lambda_l}{p\varphi_s}\int_0^{\varphi_s}\int_0^{x_r}\frac{1}{\delta}\,\mathrm{d}x\,\mathrm{d}\varphi. \tag{19}$$

The heat transfer coefficient in region 2, α_2, is assumed to be uniform. The α_2 is estimated using the following empirical equation for forced convection in internally finned tubes developed by Carnavos [10]

$$\alpha_2=0.023\frac{\lambda_l}{d_l}\left(\frac{\rho_l d_l U_l}{\mu_l}\right)^{0.8}Pr_l^{0.4}\left(\frac{A}{A_c}\right)^{0.1}\varepsilon_a^{0.5}(\sec\gamma)^3, \tag{20}$$

where $A_c=\pi(d-2h)^2/4$ is the core flow area and γ is the helix angle of the groove.

The condensation temperature difference (T_s-T_{wk}) and the heat flux q_k for region $k(=1,2)$ are obtained from

$$q_k=\left\{\frac{1}{\alpha_k}+\frac{d}{2\lambda_w}\ln\left(\frac{d_o}{d}\right)+\frac{d}{\alpha_c d_o}\right\}^{-1}(T_s-T_c)=\alpha_k(T_s-T_{wk}), \tag{21}$$

where d_o is the tube outside diameter, α_c is the coolant side heat transfer coefficient, and T_{wk} is the inside tube wall temperature for region k. Then the circumferential average heat transfer coefficient α_m is obtained from

$$\alpha_m=q_m/(T_s-T_{wm}), \tag{22}$$

where

$$q_m=\{\varphi_s q_1+(\pi-\varphi_s)q_2\}/\pi, \tag{23}$$

$$T_s-T_{wm}=\{\varphi_s(T_s-T_{w1})+(\pi-\varphi_s)(T_s-T_{w2})\}/\pi, \tag{24}$$

where q_m is the circumferential average heat flux, T_{wm} is the circumferential average wall temperature.

2.7. Modified annular flow model

The modified annular flow model is basically the same as the previous one [6] except that the expression for the interfacial shear stress is modified. In the annular flow model, the condensate generated on the fin surface

is assumed to be drained by the surface tension force toward the groove between fins. Then the condensate in the groove is forced to flow through the groove by the vapor shear force toward downstream. The condensate profile in the fin cross-section is basically the same as that for the stratified flow model shown in Fig. 1(d). The interfacial shear stress τ_i is assumed to be constant along the perimeter length. Thus τ_i is related to the frictional pressure gradient $(-dP/dz)_F$ by the following equation:

$$\tau_i = \frac{1}{S_p}\left(\frac{A}{n} - A_b\right)\left(-\frac{dP}{dz}\right)_F \cos\gamma, \tag{25}$$

where

$$A_b = 2\int_0^{x_b} \delta\, dx + \int_0^{\xi} (r_w^2 - r_b^2)\, d\beta$$

is the cross-sectional area of condensate film for a fin pitch and $S_p \approx 2(x_b + r_b\xi)$ is the perimeter length of condensate surface for a fin pitch. The $(-dP/dz)_F$ is estimated by the following correlation for microfin tubes proposed by Nozu et al. [15]:

$$\left(-\frac{dP}{dz}\right)_F = \left\{1 + (1 + 10/Fr)^{-0.5}(25X_{tt} + 1.6X_{tt}^2)\right\}_v \left(-\frac{dP}{dz}\right)_v, \tag{26}$$

where $Fr = G\chi/\sqrt{\rho_v(\rho_l - \rho_v)dg}$ is the modified Froude number, X_{tt} is the Martinelli parameter and $(-dP/dz)_v$ is the pressure gradient for single-phase vapor flow. The $(-dP/dz)_v$ is estimated by using the following correlation for internally finned tubes proposed by Carnavos [10]:

$$\left(-\frac{dP}{dz}\right)_v = 0.092 Re_v^{-0.2}\frac{1}{d_h}\frac{d_e}{d}(\sec\gamma)^{0.75}\frac{(G\chi)^2}{\rho_v}, \tag{27}$$

where d_h is the hydraulic diameter of tube.

3. Numerical results

Numerical predictions of α_m by the modified annular flow model, modified stratified flow model, previously proposed annular flow model [6] and previously proposed stratified flow model [7] are compared with available experimental data for six tubes and five refrigerants. Table 1 shows the tube and fin dimensions of test tubes used in the previous studies [6,11–14]. The fin dimensions were obtained from the enlarged photograph of the tube cross-section. Since the fin profile was somewhat different among the fins, the average value of each dimension for three to five fins was adopted as the experimental data. The test fluid was R11 for tube A, R123, R134a and R22 for tube B, R134a for tube C, R410A for tubes D and E, and R22 for tube F. The test section was basically a double-tube condenser consisting of a number of subsections. The inner tube was a microfin tube and the outer tube was a smooth tube. The refrigerant and cooling water flowed counter-currently through the test section. For each subsection the local wall temperatures at the top, side(s) and bottom of the inner tube were measured by thermocouples. In the data reduction, the physical properties of refrigerants were obtained from the REFPROP Version 6.0 [16]. The uncertainty in the measured α_m is estimated to be within 10%.

Fig. 2 shows a comparison of theoretical predictions with available experimental data for R22 condensing in a tube with $d_o = 10.0$ mm [13]. The predictions of the annular flow models are shown only for the region where the grooves are not flooded with condensate. The modified annular flow model (denoted as annular 2) gives a better agreement than the previously proposed one (denoted as annular 1). It should be noted here that this model cannot be applied to the region where the grooves are completely flooded with condensate, because it predicts a much smaller α_m than the measured value (about one half). The modified stratified flow model (denoted as stratified 2) predicts 4–8% lower α_m than the previously proposed one (denoted as stratified 1) that assumed a flat vapor–liquid interface. It is also seen that this model gives a good agreement with the measured value irrespective of χ.

Fig. 3 shows the values of φ_s and φ_f corresponding to Fig. 2 that were obtained from the previously proposed and modified stratified flow models. Both φ_s and φ_f decreases gradually as $1 - \chi$ increases. Comparison of the previously proposed model (denoted as stratified 1) and modified one (denoted as stratified 2) reveals that the values of φ_s and φ_f obtained by the latter model are 3–18° smaller than those obtained by the former model. This is consistent with the heat transfer result shown in Fig. 2, because α_1 given by Eq. (19) is much greater than α_2 given by Eq. (20).

Figs. 4–11 show comparisons of α_m between the predictions of the modified annular flow and stratified flow models and the measured value for tubes A–F. In these figures the ratio of the predicted value α_{pre} to the measured value α_{exp}, $\alpha_{m,pre}/\alpha_{m,exp}$, is plotted as a function of χ. Considering the accuracy of measured T_s and T_w, the experimental data adopted are limited to those which satisfy the condition of $T_s - T_w > 0.8$ K. As was the case for Fig. 2, the predictions of the modified annular flow model are shown only for the region where the grooves are not flooded with condensate. This model gives a good agreement (within ±20%) with most of the measured values except for tube E with R410 A (Fig. 10) and tube F with R22 (Fig. 11). For these tubes the theoretical prediction of the modified annular flow model is 6–34% higher than the measured value. The modified stratified flow model gives a good agreement

Table 1
Fin and tube dimensions

Tube designation			A	B	C	D	E	F
Outside diameter	d_o	mm	9.5	10.0	9.5	7.0	7.0	7.0
Fin root diameter	d	mm	8.44	8.48	8.88	6.50	6.49	6.50
Number of fins	n	Dimen-sionless	47	60	60	50	60	50
Helix angle	γ	Degree	20.0	18.0	18.7	18.0	18.0	12.0
Fin pitch[a]	p	mm	0.53	0.42	0.44	0.39	0.34	0.40
Fin height	h	mm	0.24	0.16	0.19	0.21	0.19	0.22
Fin half tip angle[a]	θ	Degree	30.5	19.9	22.3	19.5	13.1	12.7
Curvature radius at corner of fin tip[a]	r_0	mm	0.074	0.015	0.025	0.008	0.03	0.02
Length of flat portion at fin tip[a]	x_0	mm	0.004	0.027	0.015	0.019	0.018	0.032
Area enhancement ratio	ε_a	Dimen-sionless	1.49	1.52	1.51	1.71	1.78	1.83
Length of subsection		mm	400	500	600	300	300	1090
Tube length		m	3.2	6.0	1.2	1.8	1.8	7.56
Authors			Nozu and Honda	Haraguchi	Hayashi	Miyara et al.	Miyara et al.	Uchida et al.

[a] Dimension in a cross-section normal to groove.

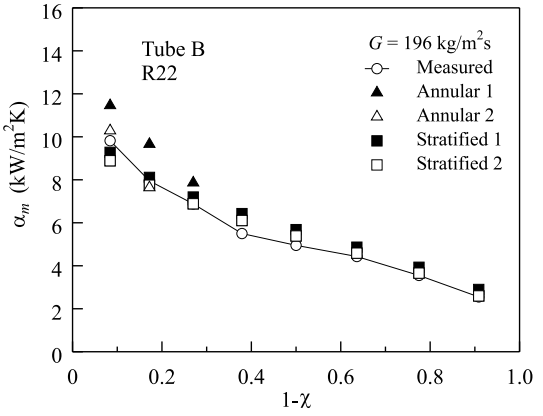

Fig. 2. Variation of α_m with $1-\chi$.

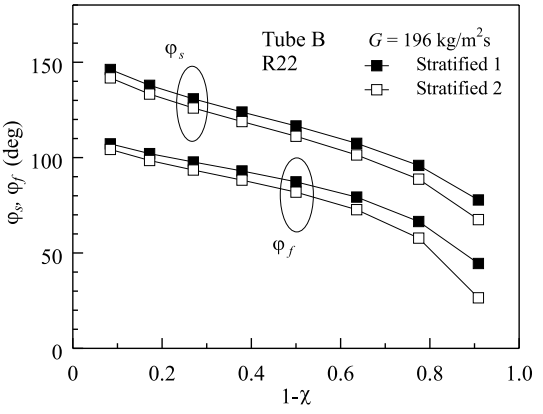

Fig. 3. Variations of φ_s and φ_f with $1-\chi$.

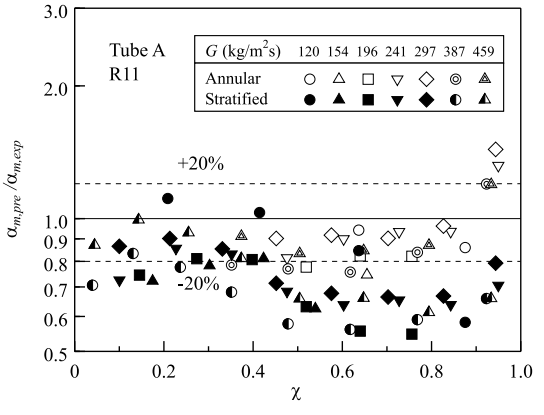

Fig. 4. Comparison of measured and predicted α_m values.

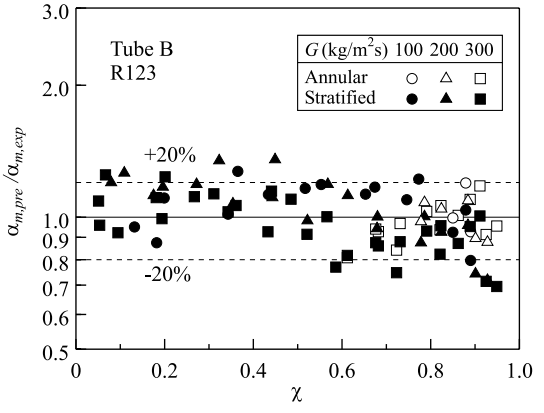

Fig. 5. Comparison of measured and predicted α_m values.

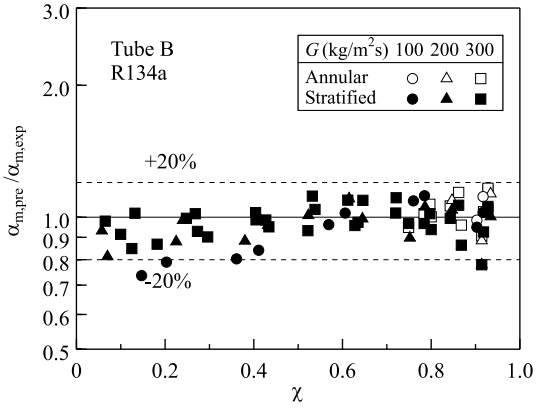

Fig. 6. Comparison of measured and predicted α_m values.

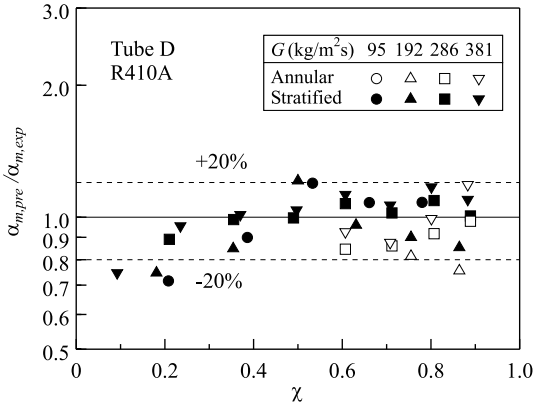

Fig. 9. Comparison of measured and predicted α_m values.

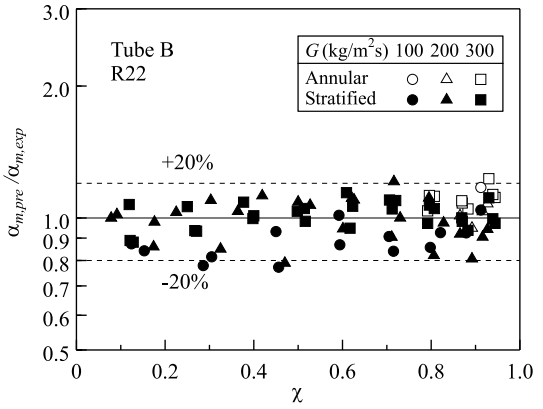

Fig. 7. Comparison of measured and predicted α_m values.

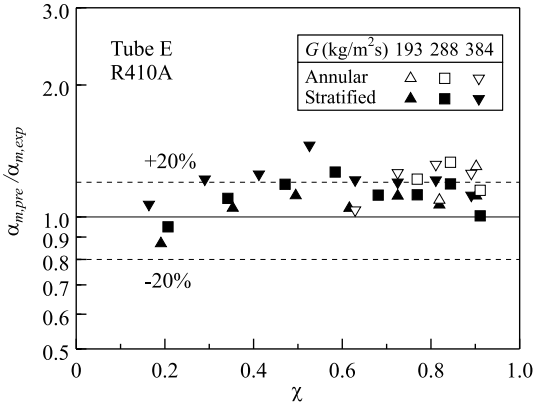

Fig. 10. Comparison of measured and predicted α_m values.

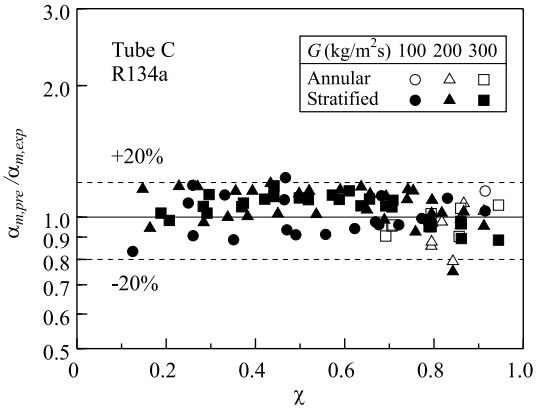

Fig. 8. Comparison of measured and predicted α_m values.

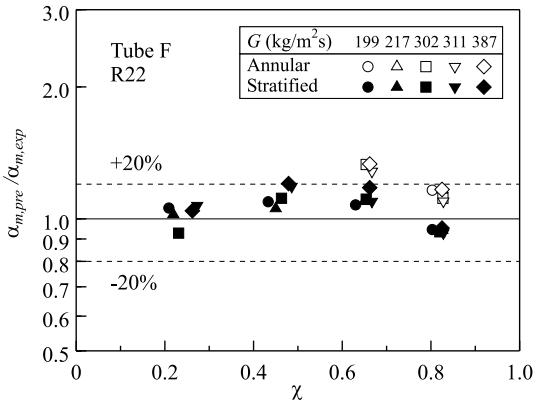

Fig. 11. Comparison of measured and predicted α_m values.

(within ±20%) with most of the measured values except for tube A with R11 (Fig. 4) and tube B with R123 (Fig. 5). For tube A with R11, this model predicts a much smaller α_m than the measured value for $\chi > 0.4$, whereas the former gives a fair agreement with the latter for $\chi < 0.4$. For tube B with R123, most of the measured values for $G = 100$ and 200 kg/m^2 s agree within ±20% with the predictions of the modified stratified flow

model. For $G = 300$ kg/m^2 s, however, the modified stratified flow model tends to underpredict the measured value at high χ. The most significant difference in the physical properties among these test fluids is the vapor density. Table 2 shows the vapor-to-liquid density ratio of the test fluids at the experimental conditions. The value of ρ_v/ρ_l increases in the order of R11, R123, R134a, R22 and R410A. It is also seen that ρ_v/ρ_l for R11 and R123 are much smaller than that for R134a, R22 and R410A. This indicates that the effect of vapor shear force on the condensation heat transfer is much stronger for the former than the latter. It is relevant to note here that the performance of the modified stratified flow model shown in Figs. 4–11 is consistent with the above discussion.

Tables 3 and 4 summarize the results of the evaluation of four theoretical models. The performance of each theoretical model was assessed in terms of the arithmetic mean error, a.m., mean absolute error, m.a., and root-mean-square error, r.m.s., defined as follows:

$$\text{a.m.} = \frac{1}{N}\sum \frac{\alpha_{m,pre} - \alpha_{m,exp}}{\alpha_{m,exp}} \times 100\%, \tag{28}$$

$$\text{m.a.} = \frac{1}{N}\sum \frac{\left|\alpha_{m,pre} - \alpha_{m,exp}\right|}{\alpha_{m,exp}} \times 100\%, \tag{29}$$

$$\text{r.m.s.} = \sqrt{\frac{1}{N}\sum \left(\frac{\alpha_{m,pre} - \alpha_{m,exp}}{\alpha_{m,exp}}\right)^2} \times 100\%, \tag{30}$$

where N is the number of data points. The data points adopted for the evaluation of the annular flow models are smaller than those for the stratified flow models. This is because only the data in which the inter-fin space is not flooded with condensate are considered. Generally, the modified annular flow model gives a better agreement with the measured value than the previously proposed one. The r.m.s. error is within 17.7% for tubes A–D, whereas it is 28.3% and 25.9% for tubes E and F, respectively. The modified stratified flow model gives a better agreement with the measured value than the previously proposed one except for tube A with R11. The r.m.s. error is within 17.7% for tubes B–F, whereas it is 29.6% for tube A.

Nozu et al. [15] have shown the photographs of condensing two-phase flow at the exit of tube A. As expected, the flow pattern of condensing two-phase flow changes as condensation proceeds. The flow pattern is the annular flow when G and χ are large, whereas it is the stratified flow when G and χ are small. Various flow patterns appear in the intermediate ranges of G and χ. Also, it should be mentioned here that the actual annular flow, is accompanied by the disturbance wave and condensate entrainment. However, comparison of the predicted and measured α_m shown in Figs. 4–11 indicates that the simplified theoretical models are very useful as far as the prediction of α_m is concerned. It is also seen that most of the measured α_m for tubes A–D are closer to the higher of the two theoretical predictions. In Table 4, one more case is also presented in which the higher of the two theoretical predictions are adopted as the calculated value. In this case a good agreement (r.m.s. error of less than 21.1%) between the theoretical prediction and the measured value is obtained for all combinations of tubes and refrigerants.

Table 2
Vapor-to-liquid density ratios of test fluids

	R11	R123	R134a	R22	R410A
T_s (K)	313	323	323	323	313
ρ_v/ρ_l	6.87×10^{-3}	9.33×10^{-3}	5.97×10^{-2}	8.00×10^{-2}	0.102

Table 3
Performance of previously proposed theoretical models[a]

Tube	Fluid	d_o	Annular flow model 1				Stratified flow model 1			
			N	a.m.	m.a.	r.m.s.	N	a.m.	m.a.	r.m.s.
A	R11	9.5	31	5.1	13.0	18.0	47	−19.2	21.7	25.2
B	R123	10.0	31	14.3	16.5	21.4	65	9.8	17.3	21.2
	R134a	10.0	23	17.8	17.8	20.8	57	1.5	7.6	9.2
	R22	10.0	24	21.6	21.6	23.2	66	3.4	8.8	10.7
C	R134a	9.5	32	16.9	17.6	20.3	78	9.2	11.4	13.7
D	R410A	7.0	15	17.3	20.4	29.7	26	5.0	11.5	13.8
E	R410A	7.0	12	44.7	44.7	46.0	23	19.1	19.4	22.0
F	R22	7.0	13	49.9	49.9	50.7	20	15.9	15.9	18.6

[a] N: number of experimental data; a.m.: arithmetic mean error (%); m.a.: mean absolute error (%); r.m.s.: root-mean-square error (%).

Table 4
Performance of modified theoretical models[a]

Tube	Fluid	d_o	Annular flow model 2				Stratified flow model 2				Annular flow model 2 + stratified flow model 2			
			N	a.m.	m.a.	r.m.s.	N	a.m.	m.a.	r.m.s.	N	a.m.	m.a.	r.m.s.
A	R11	9.5	25	−7.8	17.0	19.1	47	−26.5	27	29.6	47	−11.6	17.1	19.2
B	R123	10.0	22	−1.3	8.5	10.1	65	1.9	13.3	16.0	65	5.9	11.6	14.1
	R134a	10.0	16	3.9	8.1	9.5	57	−3.4	7.6	9.9	57	−1.3	8.0	9.9
	R22	10.0	14	8.8	9.5	11.1	66	−2.2	8.5	10.3	66	0.2	9.2	10.9
C	R134a	9.5	18	−2.7	6.9	8.8	78	4.2	9.0	10.8	78	5.7	8.5	10.2
D	R410A	7.0	10	−8.5	12.2	14.2	26	−0.9	10.7	13.3	26	−0.5	11.0	13.7
E	R410A	7.0	9	21.9	21.9	24.0	23	13.4	14.9	17.7	23	16.5	18.1	21.1
F	R22	7.0	8	20.7	20.7	22.5	20	5.2	8.9	10.1	20	13.1	13.8	16.4

[a] N: number of experimental data; a.m.: arithmetic mean error (%); m.a.: mean absolute error (%); r.m.s.: root-mean-square error (%).

4. Conclusions

Modified theoretical models of film condensation in horizontal microfin tubes have been presented. The stratified flow regime and the annular flow regime were considered. For the stratified flow regime, the previously proposed theoretical model was modified to take account of the vapor–liquid interface curvature due to the surface tension force. The profile of stratified condensate was determined by the combination of the modified Taitel and Dukler model [7] for the void fraction and the Brauner et al. model [9] for the interface curvature. For the upper part of the tube exposed to the vapor flow, the condensate film was assumed to be laminar and the heat transfer rate was calculated by the combined surface tension and gravity drained flow model. For the lower part of the tube exposed to the condensate flow, the heat transfer rate was estimated by the forced convection correlation for internally finned tubes proposed by Carnavos [10]. For the annular flow regime, the previously proposed theoretical model was modified to evaluate the interfacial shear stress more accurately. The theoretical predictions of the circumferential average heat transfer coefficient by the previously proposed and modified models were compared with available experimental data for six tubes and five refrigerants. A better agreement was obtained by the modified models as compared to the previously proposed models. The r.m.s. error was within $\pm 21.1\%$ for all cases when the higher of the two theoretical predictions was adopted as the calculated value.

References

[1] R.L. Webb, Principles of Enhanced Heat Transfer, Wiley, New York, 1994, pp. 482–505.
[2] T.A. Newell, R.K. Shah, Refrigerant heat transfer, pressure drop, and void fraction effects in microfin tubes, in: Proceedings of the 2nd International Symposium on Two-Phase Flow and Experimentation, Edizioni ETS, Italy, vol. 3, 1999, pp. 1623–1639.
[3] A. Cavallini, L. Doretti, N. Klammsteiner, G.A. Longo, L. Rosetto, Condensation of new refrigerants inside smooth and enhanced tubes, in: Proceedings of the 19th International Cong. Refrigeration, Hague, Netherland, vol. IV, 1995, pp. 105–114.
[4] N. Shikazono, M. Itoh, M. Uchida, T. Fukushima, T. Hatada, Predictive equation proposal for condensation heat transfer coefficient of pure refrigerants in horizontal microfin tubes, Trans. Jpn. Soc. Mech. Engrs. 64 (1998) 196–203 (in Japanese).
[5] C.Y. Yang, R.L. Webb, A predictive model for condensation in small hydraulic diameter tubes having axial microfins, ASME J. Heat Transfer 119 (1997) 776–782.
[6] S. Nozu, H. Honda, Condensation of refrigerants in horizontal, spirally grooved microfin tubes: numerical analysis of heat transfer in annular flow regime, ASME J. Heat Transfer 122 (2000) 80–91.

[7] H. Honda, H.S. Wang, S. Nozu, A theoretical model of film condensation in horizontal microfin tubes, in: Proceedings of the 34th Nat. Heat Transfer Conference, ASME, Pittsburgh, PA, 2000, NHTC-12213.
[8] Y. Taitel, A.E. Dukler, A model for predicting flow regime transitions in horizontal and near horizontal gas–liquid flow, AIChE J. 22 (1976) 47–55.
[9] N. Brauner, J. Rovinsky, D.M. Maron, Determination of the interface curvature in stratified two-phase systems by energy considerations, Int. J. Multiphase Flow 22 (1996) 1167–1185.
[10] T.C. Carnavos, Heat transfer performance of internally finned tubes in turbulent flow, Heat Transfer Eng. 1 (4) (1980) 32–37.
[11] M. Uchida, M. Itoh, N. Shikazono, T. Hatada, T. Ohtani, Development of high performance microfin tubes (2nd Report: Experimental study), in: Proceedings of the 31st Cond. and Refrig. Eng. Joint Conference, Tokyo, Japan, 1997, pp. 81–84.
[12] T. Hayashi, Enhancement of condensation of HFC-134a in horizontal tubes, M. Eng. Thesis, Kyushu University, 1998 (in Japanese).
[13] H. Haraguchi, Studies on condensation of HCFC-22, HFC-134a and HCFC-123 in horizontal tubes, Dr. Eng. Thesis, Kyushu University, 1994 (in Japanese).
[14] A. Miyara, K. Nonaka, M. Taniguchi, Condensation heat transfer and flow pattern inside a herringbone-type microfin tube, Int. J. Refrigeration 23 (2000) 141–152 (also private communication).
[15] S. Nozu, H. Katayama, H. Nakata, H. Honda, Condensation of a refrigerant CFC11 in horizontal microfin tubes (proposal of a correlation equation for frictional pressure gradient), Exp. Thermal Fluid Sci. 18 (1998) 82–96.
[16] M.O. McLinden, S.A. Klein, E.W. Lemmon, A.P. Peskin, NIST thermodynamic and transport properties and refrigerant mixtures – REFPROP, Version 6.0, 1998.